

## The glass-forming ability of model metal-metalloid alloys

Kai Zhang, Yanhui Liu, Jan Schroers, Mark D. Shattuck, and Corey S. O'Hern

Citation: *The Journal of Chemical Physics* **142**, 104504 (2015); doi: 10.1063/1.4914370

View online: <http://dx.doi.org/10.1063/1.4914370>

View Table of Contents: <http://scitation.aip.org/content/aip/journal/jcp/142/10?ver=pdfcov>

Published by the AIP Publishing

---

### Articles you may be interested in

[Computational studies of the glass-forming ability of model bulk metallic glasses](#)

*J. Chem. Phys.* **139**, 124503 (2013); 10.1063/1.4821637

[Local structure origin of higher glass forming ability in Ta doped Co<sub>65</sub>B<sub>35</sub> amorphous alloy](#)

*J. Appl. Phys.* **112**, 073520 (2012); 10.1063/1.4757945

[On the determination of the glass forming ability of Al<sub>x</sub>Zr<sub>1-x</sub> alloys using molecular dynamics, Monte Carlo simulations, and classical thermodynamics](#)

*J. Appl. Phys.* **112**, 073508 (2012); 10.1063/1.4756037

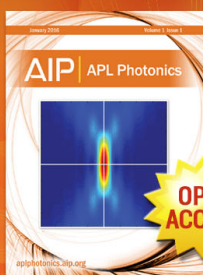
[A simple criterion to predict the glass forming ability of metallic alloys](#)

*J. Appl. Phys.* **111**, 023509 (2012); 10.1063/1.3676196

[Structural origin underlying poor glass forming ability of Al metallic glass](#)

*J. Appl. Phys.* **110**, 013519 (2011); 10.1063/1.3605510

---



Launching in 2016!

The future of applied photonics research is here

OPEN  
ACCESS

**AIP** | APL  
Photonics

## The glass-forming ability of model metal-metalloid alloys

Kai Zhang,<sup>1,2</sup> Yanhui Liu,<sup>1,2</sup> Jan Schroers,<sup>1,2</sup> Mark D. Shattuck,<sup>3,1</sup>  
 and Corey S. O'Hern<sup>1,2,4,5</sup>

<sup>1</sup>Department of Mechanical Engineering and Materials Science, Yale University, New Haven, Connecticut 06520, USA

<sup>2</sup>Center for Research on Interface Structures and Phenomena, Yale University, New Haven, Connecticut 06520, USA

<sup>3</sup>Department of Physics and Benjamin Levich Institute, The City College of the City University of New York, New York, New York 10031, USA

<sup>4</sup>Department of Physics, Yale University, New Haven, Connecticut 06520, USA

<sup>5</sup>Department of Applied Physics, Yale University, New Haven, Connecticut 06520, USA

(Received 18 December 2014; accepted 26 February 2015; published online 10 March 2015)

Bulk metallic glasses (BMGs) are amorphous alloys with desirable mechanical properties and processing capabilities. To date, the design of new BMGs has largely employed empirical rules and trial-and-error experimental approaches. *Ab initio* computational methods are currently prohibitively slow to be practically used in searching the vast space of possible atomic combinations for bulk glass formers. Here, we perform molecular dynamics simulations of a coarse-grained, *anisotropic* potential, which mimics interatomic covalent bonding, to measure the critical cooling rates for metal-metalloid alloys as a function of the atomic size ratio  $\sigma_S/\sigma_L$  and number fraction  $x_S$  of the metalloid species. We show that the regime in the space of  $\sigma_S/\sigma_L$  and  $x_S$  where well-mixed, optimal glass formers occur for patchy and LJ particle mixtures, coincides with that for experimentally observed metal-metalloid glass formers. Thus, our simple computational model provides the capability to perform combinatorial searches to identify novel glass-forming alloys. © 2015 AIP Publishing LLC. [<http://dx.doi.org/10.1063/1.4914370>]

### I. INTRODUCTION

Bulk metallic glasses (BMGs) are metallic alloys that form amorphous phases with advantageous material properties<sup>1</sup> such as enhanced strength and elasticity compared to conventional alloys<sup>2</sup> and thermal plastic processing capabilities that rival those used for polymers.<sup>3</sup> Despite enormous progress over the past 30 years in the development and fabrication of BMGs, their commercial use has been limited due to the high cost of some of the constituent elements and thickness constraints imposed by required rapid cooling. The search space for potential new BMGs is vast with roughly 46 transition metal, metalloid, and non-metal elements, which give rise to roughly  $10^3$ ,  $10^4$ , and  $10^5$  candidate binary, ternary, and quaternary alloys, respectively.

Bulk metallic glass formers can be divided into two primary classes: metal-metal (i.e., transition metal-transition metal) and metal-metalloid (i.e., transition metal-metalloid) systems. The structural and mechanical properties<sup>4–6</sup> and glass-forming ability (GFA)<sup>7</sup> of metal-metal systems are much better understood than for metal-metalloid systems. Dense atomic packing is the key physical mechanism that determines the glass-forming ability in metal-metal systems,<sup>3–6,8</sup> and thus these systems have been accurately modeled using coarse-grained, isotropic hard-sphere, and Lennard-Jones (LJ) interaction potentials.<sup>9,10</sup> Isotropic interaction potentials with non-additive repulsive core sizes, such as the Kob-Andersen model and other binary LJ-like mixtures, have been employed to describe the static structure and mechanical behavior,

but not the GFA, of metal-metalloid glasses.<sup>11,12</sup> However, since metalloid atoms form pronounced covalent interatomic bonds,<sup>13–16</sup> the atomic structure that influences glass formation is not simply described by packing efficiency of spherical atoms.<sup>17</sup> Faithfully describing covalent bonding in simulations is challenging. *Ab-initio* simulations can describe covalent bonding accurately,<sup>18</sup> but *ab-initio* simulations beyond tens of atoms in amorphous structures are not currently possible. Another possibility is simulations of embedded atom models that include pairwise interactions and energetic contributions from electron charge densities.<sup>13,19</sup> We take a simpler, geometric computational approach, where we model the covalent characteristics of metalloid atoms by arranging attractive patches on the surface of spherical particles to consider the directionality in covalently bonded structures. This *patchy particle model* has also been employed to study liquid stability,<sup>20</sup> formation of quasicrystals,<sup>21</sup> protein crystallization,<sup>22</sup> and colloidal self-assembly.<sup>23,24</sup>

Here, we perform molecular dynamics (MD) simulations of patchy and LJ particle mixtures with  $z = 3, 4, 6, 8,$  and  $12$  patches per particle that yield diamond, simple cubic (SC), body-centered cubic (BCC), and face-centered cubic (FCC) lattices in the crystalline state. We thermally quench equilibrated liquids to low temperature over a range of cooling rates and measure the critical cooling rate  $R_c$ , below which the system crystallizes. We show that the maximum GFA (minimal  $R_c$ ) for well-mixed patchy and LJ particle mixtures as a function of the atomic size ratio  $\sigma_S/\sigma_L$  and number fraction of the metalloid component  $x_S$  coincides with the

region where metal-metalloid glass-formers are observed in experiments.<sup>25,26</sup> We also employ the patchy particle model to investigate the GFA in systems that form intermetallic compounds<sup>27</sup> since these systems are difficult to crystallize using isotropic interaction potentials.

## II. METHODS

We performed molecular dynamics simulations<sup>28</sup> in a cubic box with volume  $V$  of  $N$  spherical particles of mass  $m$  decorated with  $z$  circular disks or “patches” arranged on the sphere surface with a particular symmetry. Aligned patches experience LJ attractive interactions, whereas the particles interact via short-range repulsions when patches are not aligned. The mixtures are bidisperse with diameter ratio  $\sigma_S/\sigma_L < 1$  and number fraction of small particles  $x_S$ .

The interaction potential between patchy particles  $i$  and  $j$  includes an isotropic short-range repulsive interaction and an anisotropic attractive interaction between patches,<sup>29</sup>

$$u(r_{ij}, \vec{s}_{i\alpha}, \vec{s}_{j\beta}) = u_R(r_{ij}) + u_A(r_{ij})v(\psi_{i\alpha}, \psi_{j\beta}), \quad (1)$$

where  $r_{ij}$  is the separation between particles  $i$  and  $j$ ,  $u_R(r_{ij})$  is the Weeks-Chandler-Andersen (WCA) purely repulsive potential,<sup>30</sup>  $u_A(r_{ij})$  is the attractive part of the Lennard-Jones potential truncated and shifted so that it is zero at  $r_c = 2.5\sigma_{ij}$  (Fig. 1(a)), the patch  $\alpha$  on particle  $i$  has orientation  $\vec{s}_{i\alpha} = (\sigma_i/2)\hat{n}_{i\alpha}$  with surface normal  $\hat{n}_{i\alpha}$ , and  $\psi_{i\alpha}$  is the angle between  $\vec{r}_{ij}$  and  $\vec{s}_{i\alpha}$  (Fig. 1(b)). For the patch-patch interaction, we assume

$$v(\psi_{i\alpha}, \psi_{j\beta}) = e^{-\frac{(1-\cos\psi_{i\alpha})^2}{\delta_{i\alpha}^2}} e^{-\frac{(1-\cos\psi_{j\beta})^2}{\delta_{j\beta}^2}}, \quad (2)$$

which is maximized when  $\psi_{i\alpha} = \psi_{j\beta} = 0$ .  $\delta_{i\alpha}$  gives the width of the interaction for patch  $\alpha$  on particle  $i$ . For each patch  $\alpha$ , we only include an interaction with the patch  $\beta$  that has the largest  $v(\psi_{i\alpha}, \psi_{j\beta})$ . In the large patch size limit, Eq. (2) becomes isotropic and the patchy particle model becomes

identical to the full Lennard-Jones potential. In the opposite limit, as  $\delta \rightarrow 0$ , the patchy particle potential reduces to  $u_R(r_{ij})$ . We considered particles with  $z = 3, 4, 6, 8,$  and  $12$  patches arranged on the sphere surface with trigonal, tetrahedral, simple cubic, BCC, and FCC symmetry (inset to Fig. 1(a)). For the investigations of  $AB_2$  compounds, we also considered systems with  $z_L = 12$  and  $z_S = 6$  for the large and small particles and arrangements that are compatible with the  $AB_2$  symmetry.<sup>31</sup>

To assess the glass-forming ability of patchy particle systems, we measured the critical cooling rate  $R_c$  below which crystallization begins to occur. The systems are cooled using one of two protocols: (1) the temperature is decreased exponentially in time  $T(t) = T_0 e^{-Rt}$  at reduced density  $\rho^* = N\sigma_L^3/V = 1.0$  from  $T_0/\epsilon_{LL} = 2.0$  in the liquid regime to  $T_f/\epsilon_{LL} = 0.01$  in the glassy state and (2) both the temperature and pressure  $p$  are decreased exponentially in time with  $p(t) = p_0 e^{-R_p t}$ , where  $R_p = R$ , the state point  $T_0/\epsilon_{LL}$  and  $p_0\sigma_L^3/\epsilon_{LL} = 20$  is in the liquid regime, and the state point  $T_f/\epsilon_{LL}$  and  $p_f\sigma_L^3/\epsilon_{LL} = 0.1$  is in the glassy regime. Protocol 2 was implemented for systems with  $z < 12$  to allow the system to choose a box volume most compatible with the low-energy crystal structure. The emergence of crystalline order is signaled by a strong increase of the bond orientational order parameters  $Q_6$  and  $Q_4$ <sup>32</sup> for cooling rates  $R < R_c$ . We focused on systems with  $N = 500$  particles, but also studied systems with  $N = 1372$  to assess finite-size effects.<sup>31</sup> The dynamics were solved by integrating Newton’s equation of motion for the translational and rotational degrees of freedom using Gear predictor-corrector methods with time step  $\Delta t = 10^{-3}\sigma_{LL}\sqrt{m/\epsilon_{LL}}$ .<sup>33</sup>

## III. RESULTS

In previous work,<sup>10</sup> we showed that the slowest critical cooling rates for binary hard sphere systems occur in the range  $0.8 \gtrsim \sigma_S/\sigma_L \gtrsim 0.73$  and  $0.8 \gtrsim x_S \gtrsim 0.5$ , which coincides with the parameters for experimentally observed metal-metal

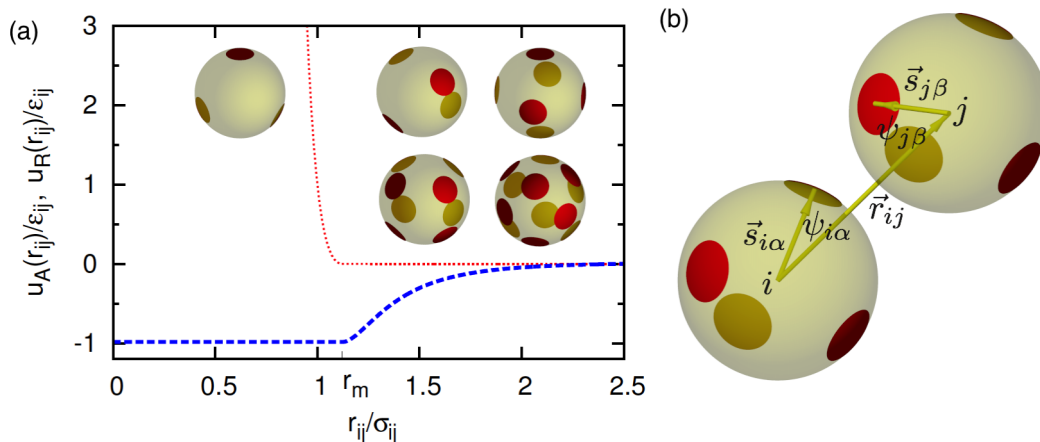


FIG. 1. (a) The purely repulsive WCA potential  $u_R(r_{ij})$  is zero for  $r_{ij} \geq r_m = 2^{1/6}\sigma_{ij}$  and the attractive part  $u_A(r_{ij})$  of the Lennard-Jones potential is truncated and shifted so that it is zero at  $r_c = 2.5\sigma_{ij}$ . Here, the Lennard-Jones energy parameters are  $\epsilon_{SS}/\epsilon_{LL} = \epsilon_{LS}/\epsilon_{LL} = 1$ . The inset shows examples of particles with 3, 4, 6, 8, and 12 patches with trigonal, tetrahedral, simple cubic, BCC, and FCC symmetry, respectively. Red patches correspond to those on the front surface of the sphere, while dark yellow patches indicate those on the back surface. (b) Definitions of quantities in the patchy particle interaction potential in Eqs. (1) and (2).

binary BMGs, such as NiNb, CuZr, CuHf, and CaAl.<sup>34–36</sup> Similar results hold for dense binary Lennard-Jones glasses with isotropic interatomic potentials.<sup>9</sup> In contrast, the metal-metalloid glass formers AuSi, PdSi, PtSi, and FeB occur at smaller  $\sigma_S/\sigma_L$  and  $x_S$ .<sup>37</sup> We present results from MD simulations that quantify the glass-forming ability of patchy particles as a function of the number of patches, their size, and placement on the sphere surface to model the GFA of metal-metalloid binary glass formers. (See Sec. II.)

We first consider monodisperse systems with  $z = 12$  patches per particle and FCC symmetry and measure the average bond orientational order parameter  $\langle Q_6 \rangle$  versus cooling rate  $R$  (using protocol 1 in Sec. II) for several patch sizes  $\delta$ . For each  $\delta$ ,  $\langle Q_6 \rangle(R)$  is sigmoidal with a midpoint that defines the critical cooling rate  $R_c$ . As  $R$  decreases toward  $R_c$ , systems with  $z = 12$  form ordered Barlow packings<sup>38</sup> and  $\langle Q_6 \rangle$  begins to increase as shown in Fig. 2. In the  $\delta \rightarrow 0$  limit,  $R_c$  converges to that for the WCA purely repulsive potential.<sup>30</sup> As the patch size increases, the 12 attractive patches promote the formation of FCC nuclei and  $R_c$  increases. For  $\delta \geq 0.05$  when patches begin to overlap,  $R_c$  begins to decrease because nucleation and growth of FCC clusters is frustrated by the concomitant formation of BCC and other types of nuclei. For sufficiently large  $\delta$ ,  $R_c$  converges to that for LJ systems. This nonmonotonic behavior for  $R_c$  versus  $\delta$  occurs for other  $z$  as well.

We now investigate the glass-forming ability at fixed patch size  $\delta = 0.1$  as a function of the number and placement of the patches for  $z = 4, 6, 8$ , and 12, which allows us to tune the crystalline phase that competes with glass formation. The GFA for  $z = 12$  and 8 is similar. As shown in Fig. 3(a),  $\langle Q_6 \rangle$  begins to increase for  $R < R_c \approx 0.04$  with the formation of FCC and BCC clusters for  $z = 12$  and 8, respectively.  $\langle Q_4 \rangle$  displays a much more modest change over the same range of  $R$ . For  $z = 4$ , the glass competes with the formation of two interpenetrating diamond lattices<sup>39</sup> (Figs. 3(b) and 3(c)),

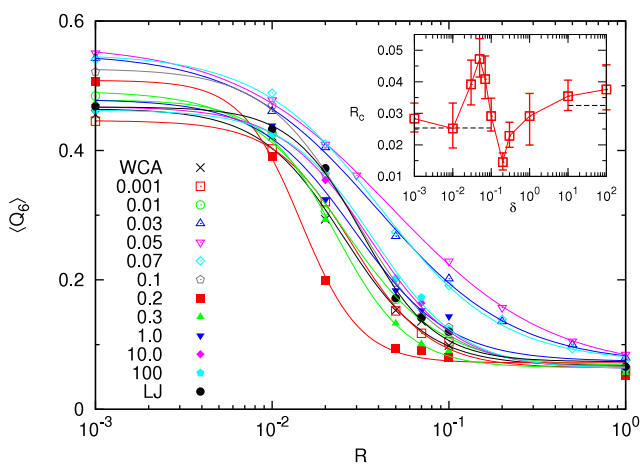


FIG. 2. The bond orientational order parameter  $\langle Q_6 \rangle$  versus cooling rate  $R$  for monodisperse patchy particles with  $z = 12$  cooled at fixed reduced density  $\rho^* = 1$  for several patch sizes  $\delta$ .  $\langle Q_6 \rangle$  was averaged over 96 separate trajectories with different initial conditions. For each  $\delta$ ,  $\langle Q_6 \rangle(R)$  was fit to a logistic function, whose midpoint gives the critical cooling rate  $R_c$ . The inset shows  $R_c$  versus  $\delta$ . The dashed horizontal lines give  $R_c$  as the patchy particle potential approaches either the LJ ( $\delta \rightarrow \infty$ ) or WCA ( $\delta \rightarrow 0$ ) limiting forms.

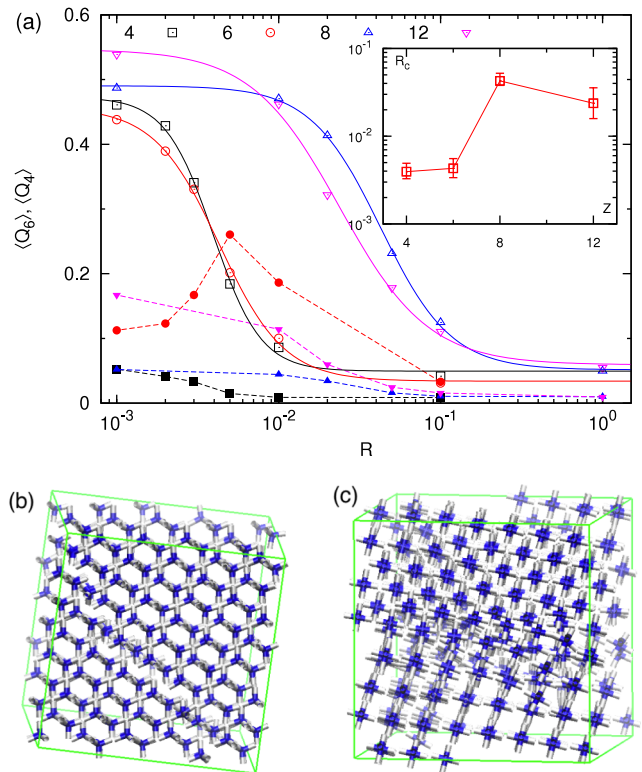


FIG. 3. (a) Average bond orientational order parameters  $\langle Q_6 \rangle$  (open symbols) and  $\langle Q_4 \rangle$  (filled symbols) versus cooling rate  $R$  for monodisperse patchy particles with  $z = 4$  (squares), 6 (circles), 8 (upward triangles), and 12 (downward triangles) and patch size  $\delta = 0.1$ . (b) and (c) Ordered configurations of patchy particles in bond representation with particles colored blue and patches white: (b) interpenetrating diamond lattices for  $z = 4$  and (c) coexistence of simple cubic and BCC lattices for  $z = 6$ .

which can be detected using either  $\langle Q_6 \rangle$  or  $\langle Q_4 \rangle$ . For  $z = 6$ , the SC phase first forms as  $R$  decreases (indicated by a strong increase in  $\langle Q_4 \rangle$ ), but as  $R$  continues to decrease BCC coexists with SC order (Fig. 3(c)), which causes  $\langle Q_4 \rangle$  to decrease and  $\langle Q_6 \rangle$  to increase. In addition, we find that systems for which the competing crystals are more open possess lower  $R_c$ .

To model metal-metalloid glass formers, we study binary mixtures of isotropic LJ particles (large metal species) and  $z = 3$  and 4 patchy particles (small metalloid species). We chose patchy particles with tetragonal (trigonal) symmetry to represent silicon (boron) atoms since they often interact with other atoms with four (three) valence electrons in  $sp^3$  ( $sp^2$ ) hybridization orbitals. The radial distribution function of simulation glass states agrees with those from experiments.<sup>31</sup> In Fig. 4(a), we show a contour plot of the critical cooling rate  $R_c$  (obtained using method 2 for cooling and measuring  $\langle Q_6 \rangle(R)$ ) for  $z = 4$  patchy and LJ particle mixtures as a function of  $\sigma_S/\sigma_L$  and  $x_S$ . We find two regions along the vertical lines  $x_S \sim 0.2$  and 0.8 with small values for  $R_c$  as determined by global measures of  $\langle Q_6 \rangle$ . However, it is also important to determine whether the patchy and LJ particles are uniformly mixed at the patchy particle number fractions  $x_S \sim 0.2$  and 0.8.

In Fig. 4(b), we characterize the solubility of the patchy particles within the matrix of LJ particles in glassy states created by rapid cooling to  $T_f$  using protocol 2 in Sec. II.

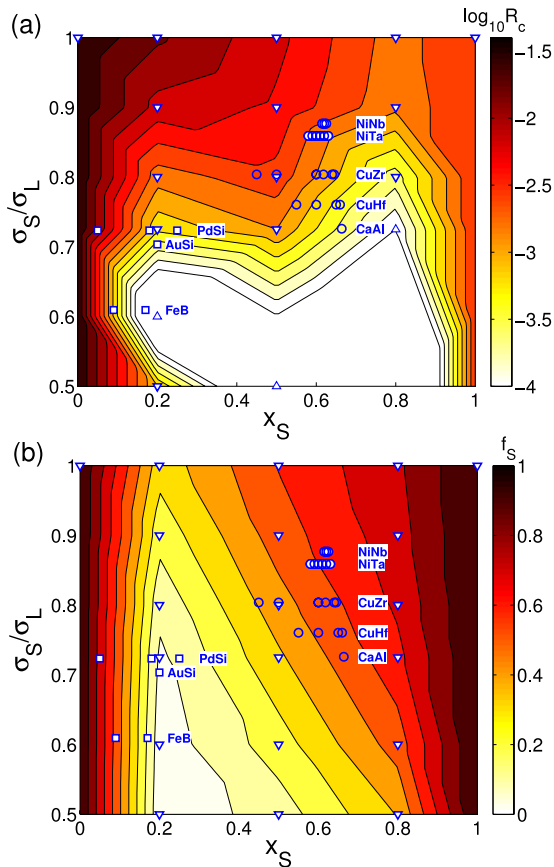


FIG. 4. (a) Contour plot of the critical cooling rate  $R_c$  versus size ratio  $\sigma_S/\sigma_L$  and small particle number fraction  $x_S$  for a binary system composed of isotropic (large) LJ particles and (small) patchy particles with  $z = 4$  and  $\delta = 0.1$ . Contours are interpolated using roughly 20 MD simulations (downward triangles) spread over parameter space. Known metal-metal and metal-metalloid binary glass-formers are indicated by circles and squares, respectively. Multiple alloy compositions are provided for each size ratio, i.e., FeB with 9% and 19% B fraction and PdSi with 5%, 20%, and 25% Si fraction. (b) Measure of the solubility ( $f_S$ ) of patchy particles within the patchy and LJ particle mixtures. Number fraction  $f_S$  of patchy particles that occur in the largest connected cluster of patchy particles from glassy configurations generated at fast cooling rates ( $R = 0.1$ ).

To quantify the solubility, for each configuration, we first determine the largest connected cluster of  $N_c$  patchy particles that share faces of Voronoi polyhedra. We then calculate the radius  $R_c$  of the sphere that  $N_c$  patchy particles would assume when confined to a sphere of volume  $4\pi R_c^3/3 = N_c/\rho_S$  at density  $\rho_S = N_S/V_S$ , where  $V_S = V x_S \sigma_S^3 / (x_L \sigma_L^3 + x_S \sigma_S^3)$  and  $V$  is the volume of the cubic simulation cell. We define the patchy particle solubility  $f_S = N_{sc}/N_S$  for each configuration, where  $N_{sc}$  is the maximum number of patchy particles that can be enclosed by a sphere of radius  $R_c$  among all possible locations centered at each of the  $N_c$  patchy particles. Small values of  $f_S$  indicate that patchy particles are more likely to be neighbors with LJ particles, not other patchy particles, while  $f_S \sim 1$  indicates all patchy particles are in a spherical aggregate.<sup>31</sup>

Although the global bond orientational order parameter  $\langle Q_6 \rangle$  indicates good glass-forming ability for LJ and patchy particle mixtures at both small ( $x_S \sim 0.2$ ) and large ( $x_S \sim 0.8$ ) fraction of patchy particles, we find that strong demixing of the patchy and LJ particles occurs for  $x_S \sim 0.8$ . Thus,

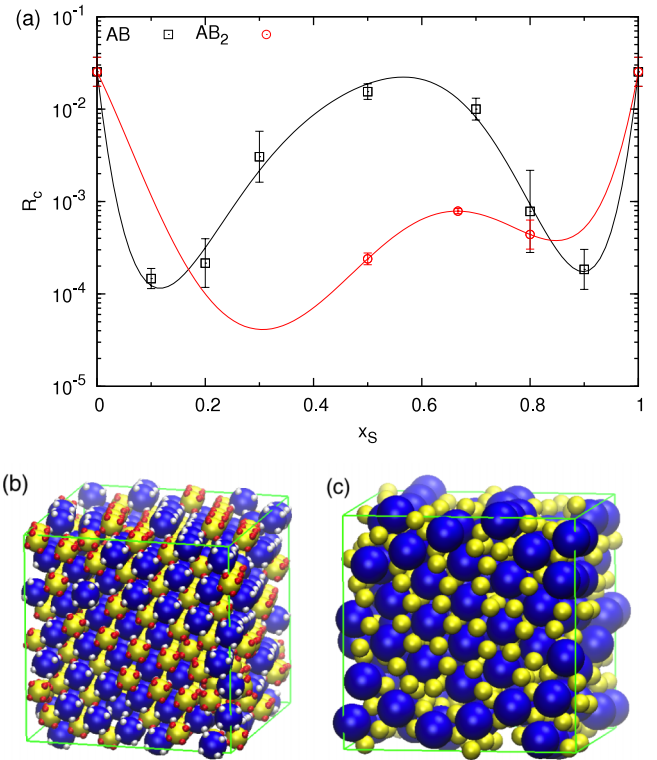


FIG. 5. (a) Critical cooling rate  $R_c$  versus  $x_S$  for model  $AB$  (squares) and  $AB_2$  (circles) intermetallic compounds. (b) and (c) Intermetallic compounds formed at cooling rate (protocol 2)  $R = 10^{-3} < R_c$ . The solid lines, which interpolate between the data points, are meant as guides to the eye. (b)  $AB$  compound with  $z_L = z_S = 8$  (patches are shown as small white and red bumps), BCC symmetry, and  $\sigma_S/\sigma_L = 0.8$ . (c)  $AB_2$  compound with  $z_L = 12$  and  $z_S = 6$  (patches not shown), stacked hexagonal planes, and  $\sigma_S/\sigma_L = 0.5$ .

when taken together, Figs. 4(a) and 4(b) show that there is only one region in the  $\sigma_S/\sigma_L$  and  $x_S$  plane where well-mixed, good glass-formers occur:  $0.2 \leq x_S \leq 0.4$  and  $0.5 \leq \sigma_S/\sigma_L \leq 0.75$ . This region in the  $\sigma_S/\sigma_L$  and  $x_S$  plane coincides with the region where binary metal-metalloid glass alloys (e.g., AuSi, PdSi, PtSi, and FeB) are observed. We also find similar simulation results for mixtures of tri-valent ( $z = 3$ ) patchy and LJ particles, which mimic FeB glass-formers.<sup>31</sup> Two amorphous alloys with metalloid fractions  $x_S < 0.2$  fall outside the optimal GFA regime for  $z = 4$  patchy and LJ particle mixtures in Fig. 4(a), i.e.,  $\text{Fe}_{91}\text{B}_9$  and  $\text{Pd}_{95}\text{Si}_5$ . However, for these alloys, the critical cooling rates are several orders of magnitude larger than those near  $x_S \sim 20\%$ .<sup>37</sup> In addition, the fact that ternary metal-metal-metalloid glass formers (CoMnB, FeNiB, FeZrB, and NiPdP), for which the metal components have similar atomic sizes, also possess metalloid number fractions  $x_S \sim 0.2$  supports our results.<sup>26</sup>

It is also difficult to capture the formation of intermetallic compounds that possess particular atomic stoichiometries in each local environment using isotropic hard-sphere or Lennard-Jones potentials. We show that crystallization of intermetallic compounds can be studied efficiently using binary mixtures of patchy particles. We focus on two model intermetallic compounds: (1) an  $AB$  compound with BCC symmetry and (2) an  $AB_2$  compound composed of hexagonal layers. We model the  $AB$  compound using a binary mixture of  $z_S = z_L = 8$  patchy particles with diameter ratio

$\sigma_S/\sigma_L = 0.8$  (Fig. 5(b)). For the  $AB_2$  compound, we consider a binary mixture of  $z_L = 12$  and  $z_S = 6$  patchy particles with  $\sigma_S/\sigma_L = 0.5$  (Fig. 5(c)). To encourage compound formation, we only include attractive interactions between patches on different particle species (with  $\delta = 0.1$ ) and repulsive LJ interactions between particles of the same type. We find that the critical cooling rate  $R_c$  has a local maximum (and glass-forming ability has a minimum) at the number fraction expected for compound formation ( $x_S = 0.5$  for  $AB$  and  $x_S = 2/3$  for  $AB_2$ ) (Fig. 5(a)). Similar results have been found for the critical casting thickness at stoichiometries that correspond to intermetallic compounds for CuZr.<sup>40</sup> For both  $AB$  and  $AB_2$ ,  $x_S \sim 0.2$  yields the smallest critical cooling rate. These results emphasize that searches for good glass-formers should avoid  $x_S$  and  $\sigma_S/\sigma_L$  combinations that yield intermetallic compound formation, which can be stable or metastable.

#### IV. CONCLUSION

We performed molecular dynamics simulations to measure the critical cooling rate  $R_c$  and assess the GFA of patchy and LJ particle mixtures. We found several key results. First, we identified nonmonotonic behavior in  $R_c$  as a function of the patch size  $\delta$ , indicating a competition between sphere reorientation and dense sphere packing in determining the GFA in the patchy particle model. Second, we tuned the number of patches per particle  $z$  and their placement on the sphere surface to vary the symmetry of the crystalline phase that competes with glass formation. We found that systems with more open lattice structures possess lower critical cooling rates. Third, we showed that the region of  $\sigma_S/\sigma_L$  and  $x_S$  parameter space where well-mixed, optimal glass-forming LJ and patchy particle mixtures occur coincides with the region where metal-metalloid glass-formers are experimentally observed. In particular, the number fraction of the metalloid species is small  $x_S \sim 0.2$ . The patchy particle model can also be employed to mimic the formation of intermetallic compounds, and our results emphasize that searches for good glass-formers should focus on stoichiometries that do not favor compound formation. In future studies, we will also measure the GFA for model glass-formers with isotropic, non-additive interaction potentials, such as Kob-Andersen potential, and compare these results to those obtained for the anisotropic, additive interaction potentials employed here.

The search for new BMGs has largely been performed using empirical rules<sup>41,42</sup> and trial-and-error experimental techniques.<sup>43</sup> Thus, only a small fraction of the search space of atomic species has been explored with fewer than 100 observed BMGs to date.<sup>44</sup> Our simple computational model for metal and metalloid atomic species provides the capability to perform more efficient and exhaustive combinatorial searches to identify novel ternary, quaternary, and multi-component glass-forming alloys. The smaller set of alloys that are predicted from simulations to possess slow critical cooling rates can then be tested experimentally using combinatorial sputtering<sup>45</sup> and other high-throughput BMG characterization techniques.<sup>40</sup>

#### ACKNOWLEDGMENTS

The authors acknowledge primary financial support from the NSF MRSEC DMR-1119826 (K.Z.). We also acknowledge support from the Kavli Institute for Theoretical Physics (through NSF Grant No. PHY-1125915), where some of this work was performed. This work also benefited from the facilities and staff of the Yale University Faculty of Arts and Sciences High Performance Computing Center and the NSF (Grant No. CNS-0821132) that in part funded acquisition of the computational facilities.

- <sup>1</sup>H. S. Chen, *Rep. Prog. Phys.* **43**, 353 (1980).
- <sup>2</sup>A. L. Greer and E. Ma, *MRS Bull.* **32**, 611 (2007).
- <sup>3</sup>J. Schroers, *Phys. Today* **66**(2), 32 (2013).
- <sup>4</sup>D. B. Miracle, *Nat. Mater.* **3**, 697 (2004).
- <sup>5</sup>H. W. Sheng, W. K. Luo, F. M. Alamgir, J. M. Bai, and E. Ma, *Nature* **439**, 419 (2006).
- <sup>6</sup>Y. Q. Cheng, H. W. Sheng, and E. Ma, *Phys. Rev. B* **78**, 014207 (2008).
- <sup>7</sup>A. Inoue, *Acta Mater.* **48**, 279 (2000).
- <sup>8</sup>R. Busch, J. Schroers, and W. H. Wang, *MRS Bull.* **32**, 620 (2007).
- <sup>9</sup>K. Zhang, M. Wang, S. Papanikolaou, Y. Liu, J. Schroers, M. D. Shattuck, and C. S. O'Hern, *J. Chem. Phys.* **139**, 124503 (2013).
- <sup>10</sup>K. Zhang, W. W. Smith, M. Wang, Y. Liu, J. Schroers, M. D. Shattuck, and C. S. O'Hern, *Phys. Rev. E* **90**, 032311 (2014).
- <sup>11</sup>W. Kob and H. C. Andersen, *Phys. Rev. E* **51**, 4626 (1995).
- <sup>12</sup>T. A. Weber and F. H. Stillinger, *Phys. Rev. B* **31**, 1954 (1985).
- <sup>13</sup>M. I. Baskes, *Phys. Rev. Lett.* **59**, 2666 (1987).
- <sup>14</sup>R. P. Messmer, *Phys. Rev. B* **23**, 1616 (1981).
- <sup>15</sup>J. F. van Acker, E. W. Lindeyer, and J. C. Fuggle, *J. Phys.: Condens. Matter* **3**, 9579 (1991).
- <sup>16</sup>C. Hausleitner and J. Hafner, *Phys. Rev. B* **47**, 5689 (1993).
- <sup>17</sup>P. F. Guan, T. Fujita, A. Hirata, Y. H. Liu, and M. W. Chen, *Phys. Rev. Lett.* **108**, 175501 (2012).
- <sup>18</sup>S. Ryu and W. Cai, *J. Phys.: Condens. Matter* **22**, 055401 (2010).
- <sup>19</sup>M. S. Daw and M. Baskes, *Phys. Rev. B* **29**, 6443 (1984).
- <sup>20</sup>F. Smalenburg and F. Sciortino, *Nat. Phys.* **9**, 554 (2013).
- <sup>21</sup>J. P. K. Doye, A. A. Louis, L. R. Lin, I. Allen, E. G. Noya, A. W. Wilber, H. C. Kok, and R. Lyus, *Phys. Chem. Chem. Phys.* **9**, 2197 (2007).
- <sup>22</sup>D. Fusco and P. Charbonneau, *Phys. Rev. E* **88**, 012721 (2013).
- <sup>23</sup>X. Mao, Q. Chen, and S. Granick, *Nat. Mater.* **12**, 217 (2013).
- <sup>24</sup>Y. Wang, Y. Wang, D. Breed, V. N. Manoharan, L. Feng, A. D. Hollingsworth, M. Weck, and D. J. Pine, *Nature* **491**, 51 (2012).
- <sup>25</sup>P. Ballone and S. Rubini, *Phys. Rev. B* **51**, 14962 (1995).
- <sup>26</sup>A. Takeuchi and A. Inoue, *Mater. Trans.* **42**, 1435 (2001).
- <sup>27</sup>T. Abe, M. Shimono, M. Ode, and H. Onodera, *J. Alloys Compd.* **434-435**, 152 (2007).
- <sup>28</sup>D. J. Evans, *Chem. Phys.* **77**, 63 (1983).
- <sup>29</sup>N. Kern and D. Frenkel, *J. Chem. Phys.* **118**, 9882 (2003).
- <sup>30</sup>J. D. Weeks, D. Chandler, and H. C. Andersen, *J. Chem. Phys.* **54**, 5237 (1971).
- <sup>31</sup>See supplementary material at <http://dx.doi.org/10.1063/1.4914370> for more details.
- <sup>32</sup>P. J. Steinhardt, D. R. Nelson, and M. Ronchetti, *Phys. Rev. B* **28**, 784 (1983).
- <sup>33</sup>M. P. Allen and D. J. Tildesley, *Computer Simulation of Liquids* (Oxford University Press, New York, 1987).
- <sup>34</sup>D. Xu, B. Lohwongwatana, G. Duan, W. L. Johnson, and C. Garland, *Acta Mater.* **52**, 2621 (2004).
- <sup>35</sup>L. Xia, W. H. Li, S. S. Fang, B. C. Wei, and Y. D. Dong, *J. Appl. Phys.* **99**, 026103 (2006).
- <sup>36</sup>Y. Wang, Q. Wang, J. Zhao, and C. Dong, *Scr. Mater.* **63**, 178 (2010).
- <sup>37</sup>Z. P. Lu and C. T. Liu, *Acta Mater.* **50**, 3501 (2002).
- <sup>38</sup>W. Barlow, *Nature* **29**, 186 (1883).
- <sup>39</sup>D. M. Proserpio, R. Hoffmann, and P. Preuss, *J. Am. Chem. Soc.* **116**, 9634 (1994).
- <sup>40</sup>Y. Li, Q. Guo, J. A. Kalb, and C. V. Thompson, *Science* **322**, 1816 (2008).
- <sup>41</sup>A. Inoue, T. Zhang, and A. Takeuchi, *Mater. Sci. Forum* **269-272**, 855 (1998).
- <sup>42</sup>W. Hume-Rothery, *The Structure of Metals and Alloys* (The Institute of Metals, London, 1950).
- <sup>43</sup>S. Ding, Y. Liu, Y. Li, Z. Liu, S. Sohn, F. J. Walker, and J. Schroers, *Nature Mater.* **13**, 494 (2014).
- <sup>44</sup>A. L. Greer, *Mater. Today* **12**, 14 (2009).
- <sup>45</sup>Y. Deng, Y. Guan, J. Fowlkes, S. Wen, F. Liu, G. Pharr, P. Liaw, C. Liu, and P. Rack, *Intermetallics* **15**, 1208 (2007).